Heliyon 9 (2023) e15408

Contents lists available at ScienceDirect

Heliyon

journal homepage: www.cell.com/heliyon

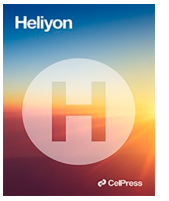

Research article

A comprehensive study of product distributions and coke deposition during catalytic cracking of vacuum gas oil over hierarchical zeolites

Jayson Fals [a,b], Carlos A.T. Toloza [c], Esneyder Puello-Polo [b], Edgar Márquez [d,**], Franklin J. Méndez [e,*]

[a] Instituto de Tecnologías del Hidrógeno y Energías Sostenibles (ITHES), UBA-CONICET, Facultad de Ingeniería, Pabellón de Industrias, Ciudad Universitaria, Ciudad Autónoma de Buenos Aires, 1428, Argentina
[b] Grupo de Investigación en Oxi/Hidrotratamiento Catalítico y Nuevos Materiales, Programa de Química-Ciencias Básicas, Universidad del Atlántico, Barranquilla, Colombia
[c] Departamento de Ciencias Naturales y Exactas, Universidad de la Costa, Barranquilla, Colombia
[d] Departamento de Química y Biología, Grupo de Investigación en Química y Biología, Facultad de Ciencias Básicas, Universidad del Norte, Barranquilla, Colombia
[e] Centro de Investigación en Ciencia Aplicada y Tecnología Avanzada, CICATA Morelos, Instituto Politécnico Nacional, Boulevard de la Tecnología 1036 Z-1 P 2/2, Atlacholoaya, 62790, Xochitepec, Mexico

ARTICLE INFO

Keywords:
Cracking
Hierarchical porosity
Vacuum gas oil
Y zeolite
Coke

ABSTRACT

In this study, zeolites (Z) were used as catalysts in the cracking of a Colombian vacuum gas oil (VGO), with a focus on product distribution and coke deposition. The catalytic tests were carried out in a MAT-type reactor under typical conditions. The zeolites were subjected to alkaline treatment with NaOH at concentrations ranging from 0.05 to 0.4 mol/L, resulting in the creation of several samples (Z-0.05, Z-0.10, Z-0.20, Z-0.30 and Z-0.40) that were then hydrothermally stabilized (Z-0.05-M, Z-0.10-M, Z-0.20-M, Z-0.30-M and Z-0.40-M) to increase mesoporosity and reduced crystallinity. The increase in mesoporosity was accompanied by an improvement in acidity. Despite Z-0.30-M having higher acidity, Z-0.00-M and Z-0.10-M exhibited the highest activity due to their high crystallinity and microporosity, yielding the highest gas yields. Gasoline was the main product, with maximum yields exceeding 30%. Z-0.20-M produced more aromatic and olefin compounds than the others, resulting in higher quality gasoline. Coke formation followed the trend: Z-0.00-M < Z-0.10-M < Z-0.20-M < Z-0.30-M. The higher intracrystalline mesoporosity in the zeolites favored the formation of a more condensed coke.

1. Introduction

The fluidized bed hydrocarbon catalytic cracking process (FCC) is considered the most important process within the refinery to convert heavy cuts into light and valuable ones. This process constantly undergoes different modifications and improvements in terms of its technology and the catalyst to increase its efficiency and meet the specific demands of each refinery [1]. The feed used in FCC

* Corresponding author.
** Corresponding author.
E-mail addresses: ebrazon@uninorte.edu.co (E. Márquez), fmendez@ipn.mx (F.J. Méndez).

https://doi.org/10.1016/j.heliyon.2023.e15408
Received 26 October 2022; Received in revised form 29 March 2023; Accepted 6 April 2023
Available online 13 April 2023

reactors is usually known as vacuum gas oil (VGO), characterized by having average boiling points of approximately 450 °C, which fall in the C20–C50 range, and the catalysts used in these units are composed of Y zeolite, which is supported on a matrix with different characteristics, active or inactive, and a binder [2–4].

The microporous nature of Y zeolites has generated some diffusive problems, conditioning the access of bulky molecules to acid sites [5]. A solution to these problems could be addressed through a zeolite leaching process in an alkaline medium, with which it is possible to remove part of the silicon from the crystalline lattice (desilication), which causes a partial destruction of the lattice, generating intracrystalline mesoporosity [6–9]. By means of this approach, it would be possible to obtain zeolites with a micropore system that provides them with adequate activity and selectivity and mesopores that facilitate diffusive processes. At the same time, on the surface of the mesopores can be carried out the pre-cracking of bulky molecules, which otherwise could not easily diffuse into the micropores. For these zeolites in which interconnected micro and mesopores coexist, their pore system is commonly said to be "hierarchical", and such a porous system has been reported to be very suitable for diverse catalytic applications [10–14]. On the other hand, given the high reaction temperatures in hydrocarbon catalytic cracking processes, zeolites undergo a deactivation process that manifests through a progressive loss of activity and/or selectivity caused by the coke deposited on the surface of the material. This formed coke is defined as the compounds with a H/C ratio = 0.3–1.0, varying substantially with the conditions under which it has been formed, such as feed properties, operating conditions, acidity, and structure porous [15]. Therefore, its characterization is essential in the FCC process.

Hydrocarbon cracking catalysts must be evaluated in the best possible way in laboratory reactors. The costs, times, and implementation should be suitable for companies in the refining or catalyst development sector, which are the applicants for this type of evaluation. In this sense, different methodologies have been developed for this purpose, including various reactor configurations and operating conditions, such as the Micro Activity Test (MAT), defined by the ASTM D-3907/03 standard. The MAT aims to approach the continuous fluidized-bed riser reactor through a fixed continuous-bed reactor [16], and its advantages are its simplicity and low cost of manufacture and operation, as well as the possibility of automation. Although the fluid dynamics are not according to the industrial process, the conversion and some selectivity data are like the plant data [17].

The activity and selectivity of a Y zeolite depend on several factors, such as its chemical composition, structure, size, and geometry of the pores. By modifying any of these properties, a zeolite with special characteristics can be produced to solve the specific needs required in each process [18–20]. In this article, the characteristics of the coke deposited on the surface of hierarchical Y zeolites were studied through catalytic cracking reactions on a MAT-type fixed bed reactor using real feeds. The effect of acid and textural properties on the distribution and quality of the products obtained were also examined. Even though there have been some studies on the desilication of Y zeolites through alkaline treatments and their use in catalysts for catalytic cracking, our main objective was to study the catalytic performance of these hierarchical zeolites and the nature of the coke deposited on their surface from cracking of a Colombian VGO in a fixed bed reactor type MAT. Most of the reported works have been carried out in the riser reactor, but we find it incredibly positive to be able to use a system that is more accessible and has a lower operating cost to study catalysts that can then be used on an industrial scale. Furthermore, knowing the optimal desilication treatment would save us time in preparing many FCC catalysts with the same zeolite load but with different desilication treatments.

2. Experimental

2.1. Reagents

A commercially protonated Y zeolite (CBV-760, Si/Al = 31) was supplied from Zeolyst International. Sodium hydroxide (reagent grade, ≥98%), hydrofluoric acid (48 wt% in H_2O, ≥99.99%), ammonium chloride (ACS reagent, ≥99.5%), chloridric acid (ACS reagent, 37%), and dichloromethane (ACS reagent, ≥99.5%), were purchased from Merck and used without further modification. N_2 (99.999% purity) was purchased from Cryogas, and the water was previously purified using a Milli-Q gradient A10 ultra-purifier.

2.2. Synthesis and characterization details

The commercial zeolite was exposed to a leaching process in an alkaline medium, known as the desilication process. Both untreated and desilicated zeolites were subjected to a stabilization process at high temperatures in the presence of water vapor. The modified and unmodified zeolites were characterized by X-ray diffraction (XRD), nitrogen physisorption, inductively coupled plasma-optical emission spectroscopy (ICP-OES), and pyridine adsorption infrared spectrometer (Py-FTIR). More details are described below.

2.2.1. Desilication process

Five NaOH solutions were selected to evaluate the alkaline concentration effect (0.05, 0.10, 0.20, 0.30, and 0.40 mol/L), obtaining 5 kinds of desilicated zeolite and identified as Z-0.05, Z-0.10, Z-0.20, Z-0.30 and Z-0.40, respectively. In a typical experiment, 5 g of zeolite dispersed in 200 mL of an aqueous NaOH solution at a known concentration was kept under magnetic stirring for 10 min at room temperature. Then the mixture was neutralized using 0.5 mol/L HCl. The obtained product was washed with deionized water and filtered under vacuum conditions.

Na^+ ions were exchanged with NH^{4+} ions using an aqueous solution of 0.50 mol/L NH_4Cl in a rotary evaporator, operating at room temperature for 8 h. The ratio between the NH_4Cl solution and the zeolite was 1 g of the solid for each 10 mL of solution. The exchanged solids were washed with deionized water and filtered under a vacuum. Then it was dried at 110 °C for 12 h and calcined at 550 °C, increasing at a linear rate of 10 °C/min from room temperature, and kept for 2 h. The efficiency of the desilication process was

calculated as the ratio between the mass of zeolite recovered after calcination and the mass of zeolite suspended in the alkaline solution. The yields varied between 75 and 85% in each leaching stage.

2.2.2. Hydrothermal stabilization

The hydrothermal treatments were carried out in a homemade tubular reactor. In a typical experiment, 3 g of zeolite was placed in the reactor and then introduced into a book-type tubular furnace. The heating process was carried out in two steps. First, a heating ramp of 5 °C/min was used until reaching a temperature of 250 °C. Once the temperature had been stabilized for 5 min, the water supply to the reactor was activated using a constant flow of close to 1.0 g/min. The heating process was continued at 10 °C/min until reaching a temperature of 780 °C. To calculate the yield, the ratio between the mass of zeolite recovered after the hydrothermal treatment and that initially loaded in the reactor was used, obtaining values greater than 95%. The zeolites desilicated with NaOH and subjected to hydrothermal stabilization were identified as Z-0.05-M, Z-0.10-M, Z-0.20-M, Z-0.30-M, and Z-0.40-M.

2.2.3. Physicochemical characterization

2.2.3.1. X-ray diffraction. The analysis was carried out using a Siemens D500 X-ray diffractometer with a CuKα monochromatic radiation source ($\lambda = 1.5418$ Å). Data were obtained in the 2θ range of 5–50° at a step size of 0.05° and a dwell time of 3 s per step. The crystallinities and unit cell sizes were calculated according to ASTM D-3906 and ASTM D-3942 standards, respectively.

2.2.3.2. Textural properties. The samples were previously degassed at 300 °C for 24 h under vacuum conditions of 10^{-6} mmHg, while the adsorption-desorption data were obtained at T = −196 °C with a 3-Flex™ automatic analyzer from Micromeritics.

2.2.3.3. Elemental analysis. The amounts of Si, Al, and Na were performed using inductively coupled plasma optical emission spectroscopy (ICP-OES). The samples were pulverized and dried for 3 h at 120 °C; then they were weighed and digested with hydrofluoric acid using a Milestone START D microwave digester. Finally, the obtained solution was filtered and diluted to a known volume with deionized water, to later be analyzed in a PerkinElmer model OPTIMA 7300 DV spectrometer.

2.2.3.4. Surface acidity. The acid sites were studied before the alkaline and hydrothermal treatment using pyridine adsorption infrared spectrometer (Py-FTIR). The wafers with a diameter of 15 mm were prepared with 80 mg of zeolite using a pressure of 4 ton/cm^2. These samples were degassed for 2 h at 450 °C and 10^{-3} Torr, the background spectrum was then recorded after cooling to room temperature. The pyridine molecules were adsorbed at 100 °C, while its desorption was carried out at 150, 300, and 400 °C. The spectra were obtained at a resolution of 4 cm^{-1} and 256 scans with a Nicolet FTIR spectrophotometer. The absorption FTIR bands at 1540 and 1450 cm^{-1} were identified as the acid Brønsted and Lewis sites by the pyridinium ion and pyridine formation, respectively [21].

Table 1
Feedstock properties: Colombian Vacuum Gas Oil.

Characteristics	Values
°API	19.7
Aniline point (°C)	78.5
CCR (wt.%)[a]	0.43
Refractive index	1.49
Distillation curve (°C)[b]	
Initial	272
10 vol %	387
30 vol %	420
50 vol %	450
70 vol %	487
95 vol %	534
Final	582
SARA fractions (wt.%)[c]	
Saturated	47.4
Aromatic	50.0
Resin	2.10
Asphaltene	0.50
Nickel (ppm)	0.48
Vanadium (ppm)	0.97
Sodium (ppm)	0.83
Iron (ppm)	0.24
Sulphur (wt.%)	1.12

[a]ASTM D-4530.
[b]ASTM D-1160.
[c]ASTM D-2007.

2.2.4. Coke characterization

2.2.4.1. Produced coke content. The coke content was evaluated using temperature-programmed oxidation (TPO), in which the carbonaceous deposits were burned in a stream of oxygen diluted in nitrogen (1% v/v). CO and CO_2 were obtained as products from the combustion, which are then converted into methane using a nickel catalyst in the presence of hydrogen, and then quantified with an FID detector. The mass balances were at least 95 wt%.

2.2.4.2. Produced coke identification. The coked zeolites were treated with hydrofluoric acid after cracking to loosen the coking compounds from the porous structure. Then, by liquid-solid extraction with dichloromethane, the soluble coke was obtained. Finally, the obtained soluble coke was analyzed by gas chromatography. These soluble structures are the coke's lightest fractions and contain most of the compounds trapped in the micropores of the zeolite. On the other hand, the background spectra obtained in Section 2.2.3.4 over the coked zeolites were also used to elucidate the nature of carbonaceous deposits. The signal at 1580 cm^{-1} was assigned to coke of aromatic nature and the signal at 1610 cm^{-1} was assigned to coke olefinic, as previously reported [22].

2.3. Catalytic tests

The catalytic cracking reactions of a Colombian vacuum gas oil (VGO) were used to evaluate the catalytic properties of selected zeolites (Z-0.00-M, Z-0.10-M, Z-0.20-M, and Z-0.30-M). The most essential characteristics of the used VGO are summarized in Table 1.

The cracking experiments were conducted in a microactivity test (MAT) unit with a fixed-bed reactor with an axial thermowell containing a thermocouple centered on the bed of materials and a bed made of quartz wool that supports the catalyst load at its midpoint. In a typical experiment, about 3 g of sample and the mass flow rate of VGO was 2.0 g/min were used. Both the feed and the amount of catalyst were kept constant, establishing the contact time as an operating variable, to vary the C/O ratio. The reaction temperature was 550 °C, and the reaction times were 20–50 s. The products generated in the process were collected at the outlet of the reactor and subsequently analyzed using a Shimadzu GC-2014 gas chromatograph equipped with an FID, a non-polar column of 30 m with a diameter of 250 μm, and a film thickness of 0.25 μm.

3. Results and discussion

3.1. Textural and crystalline properties

The textural and crystalline properties of the zeolites were evaluated before the hydrothermal stabilization treatment, and the results are shown in Table 2. The parent zeolite (Z-0.00) showed mesopores in its structure, which were generated during its manufacturing process. On the other hand, it can be observed that, as expected, the treatment with alkaline solutions proportionally increased the mesoporosity as the concentration was increased, obtaining mesopores volume from 0.136 cm^3/g (Z-0.00) to 0.534 cm^3/g (Z-0.40), generating an increase close to four times. Regarding the mesopore-specific surface area, an increase from 224 m^2/g (Z-0.00) to 458 m^2/g (Z-0.30) was also observed and then decreased to 449 m^2/g (Z-0.40). Furthermore, the average mesopore diameter increased from 26 to 59 Å, which was also proportional to the increase in the concentration of the alkaline solution. Therefore, it was clearly observed that the alkaline treatment generated an increase in mesoporosity, as well as a reduction in microporosity. This performance has been previously studied, demonstrating that a secondary porous system is generated in zeolites when they are treated with alkaline solutions [7,23–26].

The desilication process also reduced crystallinity and reached values of up to 43% compared to zeolite before treatment (Table 2). The reduction in crystallinity is explained by the loss of silicon that is part of the tetrahedral lattice with aluminum, which generates the partial elimination of the lattice. In some situations (alkalinity and zeolite class), the leached species can be incorporated again during neutralization, which generates amorphous material [7,8].

The drastic reduction that is observed in the crystallinity and microporosity values, which are generated by the treatment of the

Table 2
Textural and crystalline properties of the parent and desilicated zeolites before the hydrothermal stabilization treatment.

	Z-0.00	Z-0.05	Z-0.10	Z-0.20	Z-0.30	Z-0.40
Textural properties						
BET specific surface area (m^2/g)	943	875	836	780	737	595
Micropore specific surface area (m^2/g)	719	629	512	461	279	146
Mesopore specific surface area (m^2/g)	224	246	324	319	458	449
Total pore volume (cm^3/g)	0.618	0.606	0.643	0.664	0.701	0.732
Micropore volume (cm^3/g)	0.482	0.353	0.302	0.252	0.203	0.198
Mesopore volume (cm^3/g)	0.136	0.253	0.341	0.412	0.498	0.534
Average mesopore diameter (Å)	26	29	43	49	56	59
Crystalline properties						
Crystallinity (%)	100	84	75	72	51	43
Unit cell size (Å)	24.24	24.25	24.26	24.28	24.27	24.29
Si/Al	31.0	29.2	27.6	26.8	24.2	23.3

zeolites with the highest concentrations of NaOH evaluated, become a negative factor for the use of these catalysts in industry, due to the reduction of their catalytic activity. Furthermore, an increase in the unit cell size was also observed as the NaOH concentration in the solution increased (Table 2), which can be explained due to the loss of silicon from the tetrahedral structure. The preferential loss of silicon generates a reduction in the Si/Al ratio in the crystal lattice causing an increase in the unit cell size, this is due to the difference between the Al–O bond lengths (1.73 Å) and Si -O (1.61 Å) [6,27–29].

The textural and crystalline properties of the zeolites after hydrothermal stabilization are reported in Table 3. The results showed an additional reduction in both crystallinity and specific surface area. This reduction was more drastic in the desilicated samples than in the parent zeolite. This effect can be explained since the desilication generates a partial destabilization of the crystal lattice, which can be accompanied by a significant dealumination that affects the crystallinity and specific surface of the materials. On the other hand, the hydrothermal treatment did not generate significant changes in the unit cell size and Si/Al values, because the zeolites in their manufacture have been hydrothermally treated [6,30]. Similar behaviors have been evidenced in previous works, showing that hydrothermally treating desilicated zeolites reduces a reduction in the stability of the materials subjected to alkaline treatment, which affects their structural and acid properties compared to the original [8,31].

3.2. Acid properties

The acidity features were determined using the pyridine adsorption technique, and the results are shown in Tables 4 and 5. The strength of the acid sites was classified based on the pyridine desorption temperature (150, 300, and 400 °C) because it is well-known that there is a direct relationship between the strength of the acid site and the temperature required for the desorption of the absorbed pyridine molecules [32]. The acid sites obtained from the pyridine-adsorbed peaks at 150 °C were regarded as the total acid quantity, while the peak at 300 °C referred to the medium and strong acidity, and the desorption at 400 °C referred to the strong acid sites.

Table 4 shows the acidity distribution in the zeolites, parent and modified, without hydrothermal treatment, according to their nature and acid strength. The treated zeolites showed an increase in acidity as the hydroxide concentration increased, except for Z-0.40, this increase was generated in both acid sites when the samples are compared with the parent material. Similar results have been previously reported. Fals et al. [33] modified Y zeolite through alkaline treatment and achieved an increase in acidity greater than 50%, while Garcia et al. [34] obtained an increase of up to 60%. The maximum acidity values were obtained for the Z-0.30 zeolite; the total acidity observed doubled the value for the zeolite without treatment. Regarding Z-0.40, a reduction in the acidity value is evidenced compared to the Z-0.30 one. Sadowska et al. previously reported that the strong destruction and destabilization of the structure are caused by the alkaline treatment process itself [35].

Table 3 shows that under mild alkaline conditions (0.05, 0.10, and 0.20 mol/L NaOH), the reduction in crystallinity was not more significant than 50%, under these conditions the increase in acidity is related to the selective removal of silicon from the crystal lattice, which generated a decrease in the Si/Al ratio. Z-0.10 and Z-0.20 showed a similar Si/Al ratio. However, Z-0.20 showed a higher absolute acidity value, which together with a higher mesoporosity, makes it attractive for use as a catalyst in various processes. Z-0.40, which was treated under more severe conditions, had higher acidity than the untreated zeolite. Still, its acidity value was like the Z-0.20, which explains the reduction in its crystallinity. The latter seems to have a more significant effect on acidity than the increase in the amount of aluminum per unit cell or the formation of acidic species outside the network, which explains the similarity in acidity values when compared to the Z-0.20.

The distribution of acid sites in the zeolites, both parent and modified, after their hydrothermal stabilization, is reported in Table 5. It is shown that the B/L ratio, which corresponds to the total acid sites (after desorption of pyridine at 150 °C) and hydrothermal treatment, is similar in most of the modified materials, except Z-0.40-M. Furthermore, as expected, the variation in acidity between the base zeolite and modified ones (except for Z-0.40-M) was more significant for the Brønsted-type acid sites. However, the results showed a significant increase in the density of Lewis acid sites. The total amount of Brønsted acidity, expressed by the desorption of pyridine at a temperature of 150 °C, increased from 15 μmol/g in Z-0.00-M to 38 μmol/g in Z-0.30-M, while an increase in Lewis acid sites from 18 to 34 μmol/g was also observed. Although the ratio of Brønsted and Lewis acid sites (B/L) is very similar in the modified zeolites, a significant difference can be observed in the absolute acidities (μmolPy/g), with higher concentrations of Brønsted and Lewis acid sites

Table 3
Textural and crystalline properties of the parent and desilicated zeolites after the hydrothermal stabilization treatment.

	Z-0.00-M	Z-0.05-M	Z-0.10-M	Z-0.20-M	Z-0.30-M	Z-0.40-M
Textural properties						
BET specific surface area (m^2/g)	712	687	622	614	473	449
Micropore specific surface area (m^2/g)	501	413	315	248	162	137
Mesopore specific surface area (m^2/g)	211	274	307	366	311	312
Total pore volume (cm^3/g)	0.533	0.558	0.611	0.636	0.652	0.681
Micropore volume (cm^3/g)	0.267	0.261	0.242	0.133	0.140	0.113
Mesopore volume (cm^3/g)	0.266	0.297	0.369	0.503	0.512	0.568
Average mesopore diameter (Å)	53.1	56.4	59.5	67.2	84.7	95.4
Crystalline properties						
Crystallinity (%)	98	76	65	61	40	32
Unit cell size (Å)	24.24	24.23	24.24	24.24	24.25	24.26
Si/Al	31.0	27.6	26.4	25.9	23.7	22.8

Table 4
Acid site distributions ($\mu mol_{Py}/g$) as a desorption temperature function determined by Py-FTIR in parent zeolite and desilicated zeolites before the hydrothermal stabilization treatment.

Sample	150 °C			300 °C			400 °C		
	B	L	B/L	B	L	B/L	B	L	B/L
Z-0.00	19	23	0.8	11	16	0.7	6	11	0.5
Z-0.05	26	30	0.9	14	22	0.6	5	10	0.5
Z-0.10	29	33	0.9	17	27	0.6	11	15	0.7
Z-0.20	34	38	0.9	18	34	0.5	14	20	0.7
Z-0.30	39	39	1.0	12	17	0.7	7	9	0.8
Z-0.40	30	27	1.1	19	20	1.0	5	7	0.7

B: Brønsted sites, L: Lewis sites.

Table 5
Acid site distributions ($\mu mol_{Py}/g$) as a desorption temperature function determined by Py-FTIR in parent zeolite and desilicated zeolites after hydrothermal treatment.

Samples	150 °C			300 °C			400 °C		
	B	L	B/L	B	L	B/L	B	L	B/L
Z-0.00-M	15	18	0.8	9	13	0.7	5	9	0.6
Z-0.05-M	19	19	1.0	11	17	0.6	4	8	0.5
Z-0.10-M	24	25	1.0	14	20	0.7	8	12	0.7
Z-0.20-M	30	30	1.0	13	28	0.5	11	17	0.6
Z-0.30-M	38	34	1.1	9	10	0.9	5	7	0.7
Z-0.40-M	24	33	0.7	13	17	0.8	4	6	0.7

B: Brønsted sites, L: Lewis sites.

in Z-0.20-M. The difference between Z-0.00-M and Z-0.20-M was more significant for Brønsted acid sites, as expected, given the higher selectivity of the desilication process to removing silicon from the zeolite crystal lattice.

Leaching carried out on materials with alkaline solutions can induce a reduction in the Si/Al ratio and an increase in the number of Brønsted-type acid sites due to the elimination of silicon from the zeolite crystal lattice. The presence of aluminum atoms in the tetrahedral network of the zeolite creates a charging defect that is counteracted by the introduction of compensating cations. These cations are exchanged for protons, generating Brønsted acid centers. The proton is connected to the oxygen atom belonging to the neighboring silicon and aluminum atoms, generating an acidic hydroxyl group. The number of total Brønsted acid sites depends on the aluminum concentration in the lattice. Thus, the greater the amount of aluminum present in the structure, the greater number of Brønsted acid sites it may possess. Through the desilication treatment, some silicon is removed from the crystalline lattice, which generates an increase in the aluminum concentration in the lattice (lower Si/Al ratio) and consequently a higher density of Brønsted acid sites [30,34]. However, a considerable increase in the number of Lewis acid sites was also evidenced after desilication, as reported in previous works [36–38]. This can be explained by the leaching of some aluminum atoms that are part of the crystal lattice and

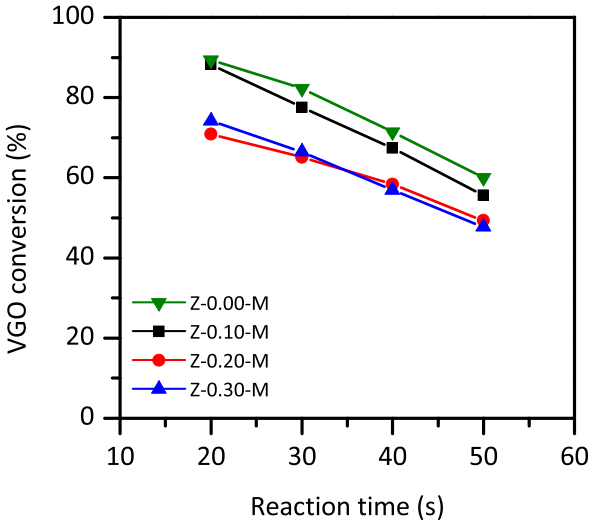

Fig. 1. VGO conversion at 550 °C as a reaction time function.

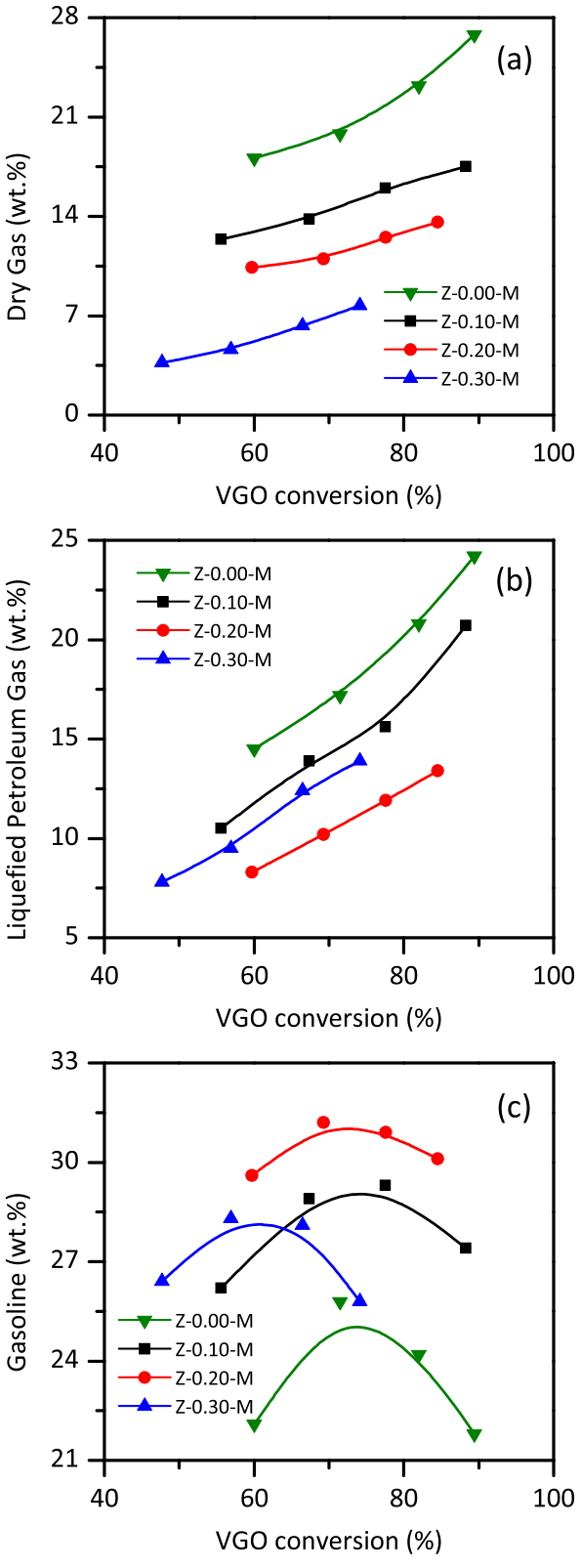

Fig. 2. Selectivity as a VGO conversion function to the formation of (a) dry gas, (b) liquefied petroleum gas, and (c) gasoline.

deposited as an amorphous material, generating extra-lattice aluminum species with the nature of Lewis acids [30,39].

3.3. Catalytic performance

The catalytic tests were performed using four selected zeolites (Z-0.00-M, Z-0.10-M, Z-0.20-M, and Z-0.30-M) to evaluate their performance in the cracking of a Colombian Vacuum Gas Oil. The characteristics of the feedstock are presented in Table 1. Although the experimental conditions were not completely consistent with the MAT technique (ASTM D-3907-03), they were adjusted to obtain suitable operating conditions to achieve the objectives of this study and to validate the results with those obtained from other experimental devices used in the catalytic cracking of hydrocarbons.

The VGO conversion (X) at 550 °C as a reaction time function was expressed as the sum of the products obtained during the process (see Eq. (1)); the products included dry gas (C1–C2), liquefied petroleum gas (C3–C4), gasoline (C5-216 °C), and coke, which is the solid residue left after the cracking reaction. The results are shown in Fig. 1.

$$X = Y_{DG} + Y_{LPG} + Y_{GASOLINE} + Y_{COKE} \quad \text{Eq. 1}$$

The VGO conversion curves show a negative slope, which can be attributed to the continuous use of the MAT fixed-bed reactor with a constant decrease in the C/O ratio. Furthermore, some differences were observed among the tested zeolites. Z-0.00-M and Z-0.10-M exhibited higher activity. Z-0.20-M and Z-0.30-M showed similar conversion values, despite Z-0.30-M having higher acidity compared to Z-0.00-M and Z-0.10-M. It is well known that an excessive loss of crystallinity and microporosity during the alkaline treatment of zeolites can have negative effects on their potential use as a catalyst. Therefore, it is important to understand the acid properties of zeolites, as both acidity and accessibility of active sites influence their catalytic performance. The generation of intracrystalline mesoporosity improves the diffusive transport of bulky molecules to the catalytic sites located inside the zeolite crystals, and zeolites with the greatest microporosity experience a confinement effect that increases the reactivity of the molecules due to the interactions that occur in the zeolite channel system.

The products generated as a function of VGO conversion during the cracking tests are shown in Fig. 2. This figure illustrates the production of dry gas (Fig. 2a), liquefied petroleum gas (Fig. 2b), and gasoline (Fig. 2c). As can be seen, dry gas and liquefied petroleum gas exhibit secondary product behavior. This can be explained by the high VGO conversion by parent and modified zeolites at low operation times, which causes significant cracking of the feed and over-cracking of heavier cuts. The results also show that Z-0.00-M and Z-0.10-M produced the highest gas yields (Dry and Liquefied Petroleum Gas), with Z-0.00-M being the highest producer of gas. Both zeolites have a higher micropore volume compared to Z-0.20-M and Z-0.30-M, and lower density of acid sites. The combination of their structural and acidity properties favors selectivity in over-cracking heavier species. On the other hand, intermediate species may adsorb in the microporous channels of the zeolites and undergo an electronic confinement effect caused by the high field gradients present inside the channels. This effect produces a contraction of the orbitals of the molecule housed inside the channels, causing a change in energy levels and an increase in the energy of the frontier orbitals, which leads to the pre-activation of the molecule. This phenomenon could cause an increase in the strength of the acid site due to acting in a confined space, and therefore, intermediates species could diffuse slowly out of the pores and crack into gas [40]. Modified zeolites with lower microporosity (Z-0.20-M and Z-0.30-M) did not exceed 15% of gas production even at VGO conversions greater than 80%, while higher microporosity zeolites (Z-0.00-M and Z-0.10-M) yielded between 12 and 20%. These values are within the range reported in previous works using MAT-type fixed-bed reactors [41].

The gasoline production decreases at high conversions after reaching a maximum (see Fig. 2c). This can be attributed to the fact that at low interaction times, the feed entering the reactor encounters the catalyst at its maximum catalytic activity. However, at a higher time, the catalyst deactivates significantly, reducing gasoline production. This behavior can be explained by the increase in coke formation, which leads to reduced conversion. In addition to the catalyst deactivation by coke deposition, the figure also shows the presence of an over-cracking effect of gasoline, as evidenced by the secondary nature of gas production. Nevertheless, gasoline was the most important product in all cases, with production ranging between 26 and 32%. Z-0.20-M exhibited the highest gasoline yields, with maximum values exceeding 32% and close to typical values obtained on an industrial scale. This sample has the highest density of acid sites and a total volume of pores mainly constituted by mesopores, which are typical characteristics of cracking catalysts designed for gasoline production. Myrstad and Engan previously reported gasoline yields of between 45 and 50% for a residue conversion between 72 and 83%, using a similar MAT reactor [42]. Although Z-0.00-M exhibited the highest conversion and gas production, its selectivity towards gasoline was lower compared to the modified zeolites. This could be due to its low mesoporosity, which does not favor hydrocarbon production in the C5–C12 range, including the aromatic species that are part of the gasoline cut.

Hydrocarbon distribution in the gasoline boiling range at iso-conversion is shown in Table 6. The composition of the gasoline cut is

Table 6
Gasoline composition at a 75% VGO conversion.

	Z-0.00-M	Z-0.10-M	Z-0.20-M	Z-0.30-M
Paraffins	23.6	22.8	8.1	11.5
Olefins	23.5	29.8	39.1	36.9
Naphthenes	20.5	13.3	12.6	16.4
Aromatics	32.4	34.1	40.2	35.2
RON	80	82	88	85

decisively in establishing its quality as a fuel and is expressed as a function of the octane number (RON). It was shown that the properties of the zeolites influenced the composition and quality of the cut. The gasoline produced with Z-0.20-M showed better quality than that compared to the produced with Z-0.00-M and the other modified zeolites, as indicated by its higher RON value. Its better quality as fuel was related to its high content of olefins and aromatics, and its lower content of paraffin. Z-0.00-M showed the highest contribution to aliphatic hydrocarbons in the gasoline range, corresponding to their higher degree of microporosity that favors terminal chain cracking reactions.

Coke production increased as a function of VGO conversion, as shown in Fig. 3. Although conversion decreases with reaction time in a fixed bed reactor, coke production increases because this compound is permanently deposited on the surface of the zeolite. The obtained coke yield was higher than that reported in the literature for both industrial processes and laboratory tests [43]. Factors such as feedstock nature, operational conditions, and zeolites properties determine the yield and characteristics of the carbonaceous deposits. Coke production under the used reaction conditions suggests that it is affected by the operating conditions and design. In the catalytic bed, a high amount of coke is generated at the beginning and in the axial profiles. This is explained by the constant and new feeding onto the bed, which, being fixed, causes irregular homogeneous deactivation. Moreover, the nature of the acid sites is crucial in coke production, as higher mesoporosity in the zeolite would facilitate the formation of a more condensed coke. Z-0.20-M and Z-0.30-M showed the highest coke production at similar conversion. Furthermore, the higher density and strength of acid sites in these zeolites caused strong adsorption of the coke precursor species, thus favoring reactions leading to its formation, such as oligomerization, hydrogen transfer, and condensation.

Fig. 4 shows the combustion profiles of the coke deposited on the surface at a VGO conversion of ca. 75%. In all the combustion profiles, the main peak can be observed at temperatures above 450 °C. Furthermore, a shoulder can be observed at low temperatures, between 200 and 450 °C. The proportion of this shoulder about to the total area under the combustion profiles was higher in Z-0.10-M. The peak at low temperatures could be attributed to coke made up of compounds with little condensation development, such as aliphatic and aromatic species with a higher H/C ratio. The peaks at high temperatures (>450 °C) could correspond to compounds with a higher degree of condensation (low H/C ratio), consisting of condensed dienes and polycondensed aromatic structures. Z-0.00-M (460 °C) and Z-0.10-M (470 °C) showed significantly lower combustion temperatures than those of Z-0.20-M (565 °C) and Z-0.30-M (545 °C). This behavior could be due to the higher density and strength of acid sites in zeolites with a higher degree of mesoporosity, which promotes the reactions that favor the formation of a much more condensed coke that burns at much higher temperatures.

Table 7 shows the relative intensities of the bands at 1580 and 1610 cm^{-1} observed from FTIR spectra of coked zeolites at a VGO conversion of ca. 75%. Both types of coke were deposited on all the coked zeolites. The aromatic nature of the coke prevailed in all the zeolites, especially in the coke formed on the zeolites with higher mesoporosity. These results are consistent with the combustion profiles for Z-0.20-M and Z-0.30-M (Fig. 4), where a more outstanding contribution of the combustion peaks was observed at higher temperatures (>500 °C). The relative intensities of the bands at 1580 and 1610 cm^{-1}, observed in Z-0.00-M and Z-0.10-M, were lower in both the aromatic and olefinic coke.

Fig. 5 shows the main compounds of the soluble coke fraction in the coked zeolites. The identified compounds of the coke fraction were aromatic species of one, two, three, and four rings, named B1, B2, B3, and B4, respectively. Zeolites with a higher degree of microporosity (Z-0.00-M and Z-0.10-M) showed a higher presence of mono- and di-aromatic species and little presence of polyaromatic compounds. Z-0.10-M had the following composition: B4 = 15 wt%, B1 + B2 = 55 wt%, and B3 = 30 wt%.The formed coke with Z-0.20-M and Z-0.30-M was more condensed, with a higher content of polyaromatic compounds. Z-0.30-M had the following distribution of compounds: B4 = 60 wt%, B1 + B2 = 20 wt% and B3 = 20 wt%. The zeolites were desactivated mainly because of the blockage of the micropores by the coke deposited inside, which allowed the deposition of polyaromatic structures that were the majority in the

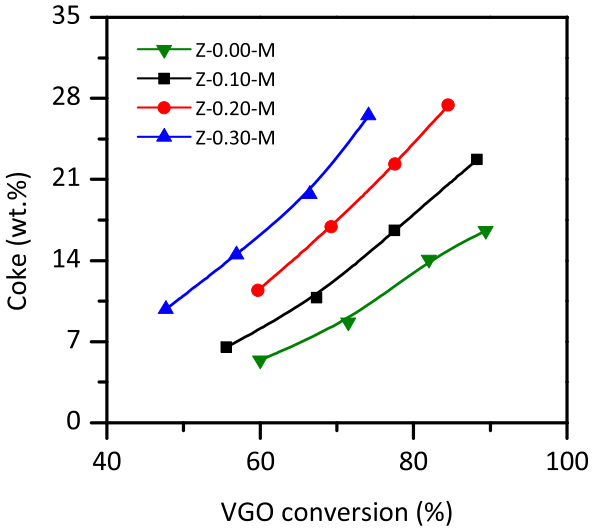

Fig. 3. Coke formation as a VGO conversion function.

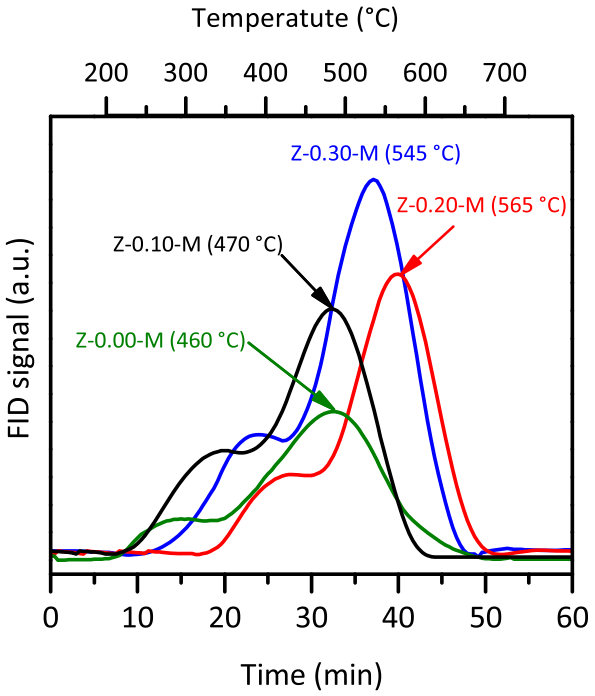

Fig. 4. TPO profiles of the coke combustion deposited on the spent catalyst at VGO conversion at about 75%.

Table 7
Relative intensities of the FTIR bands corresponding to aromatic and olefinic coke formed during the conversion of a Colombian VGO.

Signal	Z-00-M	Z-010-M	Z-0.20-M	Z-0.30-M
Aromatic band (1580 cm^{-1})	1.70	1.91	3.82	3.53
Olefinic band (1610 cm^{-1})	0.98	1.10	2.15	2.81

coke soluble in dichloromethane. This internal coke deposition was mainly attributable to the condensation of cracking products, among which the ability of olefins to form aromatics is well known through isomerization, cyclization, and condensation steps. In this sense, Z-0.20-M and Z-0.30-M had the highest content of olefins and aromatics that favored the formation of a more condensed coke than the Z-0.00-M. The results were consistent with those observed in the combustion profiles (Fig. 4) and the intensities of the bands obtained by FTIR (Table 7).

4. Conclusions

The characterization of the zeolites, subjected to leaching treatment, showed notable differences in their textural and acid properties, with a gradual increase in mesoporosity as a function of the concentration of the alkaline solution. The variation in Si/Al ratio resulting from the desilication process led to an increase in both Brønsted and Lewis acid sites. However, the zeolites subjected to more rigorous alkaline treatment suffered from excessive loss of crystallinity and microporosity, which negatively affected their catalytic performance. Z-0.00-M and Z-0.10-M had the highest gas yields, producing dry and liquefied petroleum gas, with a greater micropore volume than Z-0.20-M and Z-0.30-M. Despite having a lower density of acid sites, they had a more significant presence of strong acid sites, which could favor the selective over-cracking of heavier species. Gasoline production declined after reaching a maximum peak at high conversions. Catalyst deactivation increased due to increased coke production at high conversions. Z-0.20-M showed better gasoline cut quality (RON = 88) due to its high content of olefins and aromatics and lower content of paraffins.

The nature of the acid sites was decisive in the coke production, just as a greater mesoporosity in the zeolite facilitates the formation of a more condensed coke. Z-0.20-M and Z-0.30-M presented the highest coke production and the highest degree of condensation. The combustion profiles of the coke deposited on the surface of Y zeolites showed notable differences in their combustion peaks with shifts at higher temperatures in the case of Z-0.20-M. This differential behavior in coke burning is attributed to the different levels of difficulty in its combustion, given the composition of the deposited coke and the degrees of mesoporosity of the zeolites. The coke formed on the surface of all the zeolites showed both aromatic and olefinic nature. However, the aromatic nature prevailed in all cases, especially in the coke formed on Z-0.20-M.

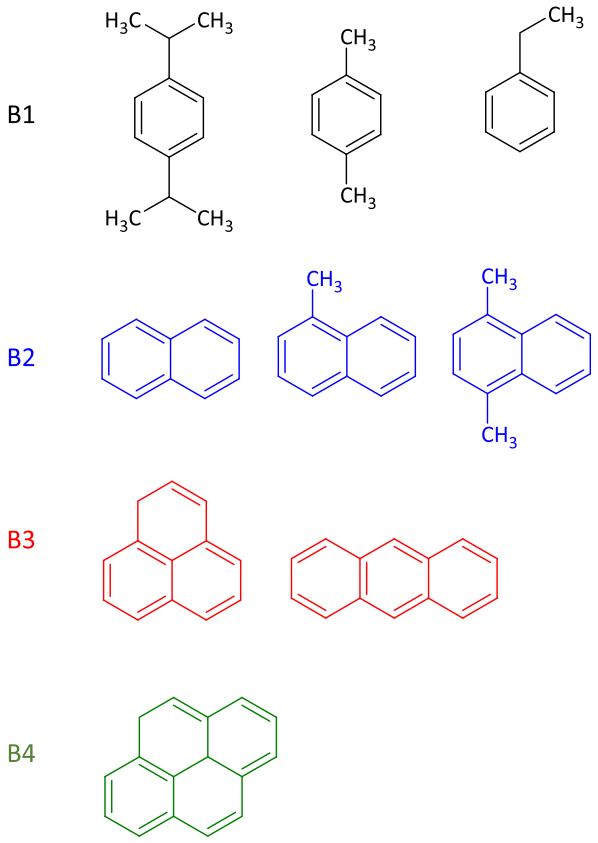

Fig. 5. Main compounds identified and quantified in the soluble coke fraction.

Author contributions statement

Jayson Fals: Performed the experiments; Analyzed and interpreted the data; Wrote the paper. Carlos A.T. Toloza, Esneyder Puello-Polo, Edgar Márquez: Conceived and designed the experiments; Contributed reagents, materials, analysis tools or data. Franklin J. Méndez: Conceived and designed the experiments; Analyzed and interpreted the data; Wrote the paper.

Data availability statement

Data will be made available on request.

Declaration of competing interest

The authors declare that they have no known competing financial interests or personal relationships that could have appeared to influence the work reported in this paper.

Acknowledgments

The authors thank the Universidad de la Costa (Barranquilla, Colombia) for funding the experimental part through the INV.100-01-001-16 project. We also give a special acknowledgment to Universidad del Atlántico and Universidad del Norte for also supporting this project.

References

[1] A. Oloruntoba, Y. Zhang, C.S. Hsu, State-of-the-art review of fluid catalytic cracking (FCC) catalyst regeneration intensification technologies, Energies 15 (2022) 2061, https://doi.org/10.3390/en15062061.
[2] M.L. Fernández, A. Lacalle, J. Bilbao, J.M. Arandes, G. de la Puente, U. Sedran, Recycling hydrocarbon cuts into FCC units, Energy Fuels 16 (2002) 615–621, https://doi.org/10.1021/ef010184i.
[3] A. Devard, G. de la Puente, U. Sedran, Laboratory evaluation of the impact of the addition of resid in FCC, Fuel Process. Technol. 90 (2009) 51–55, https://doi.org/10.1016/j.fuproc.2008.07.009.

[4] J. Fals, J.R. García, M. Falco, U. Sedran, Performance of equilibrium FCC catalysts in the conversion of the SARA fractions in VGO, Energy Fuels 34 (2020) 16512–16521, https://doi.org/10.1021/acs.energyfuels.0c02804.

[5] S. Al-Khattaf, H. de Lasa, The role of diffusion in alkyl-benzenes catalytic cracking, Appl. Catal., A 226 (2002) 139–153, https://doi.org/10.1016/S0926-860X(01)00895-X.

[6] K.P. de Jong, J. Zečević, H. Friedrich, P.E. de Jongh, M. Bulut, S. van Donk, R. Kenmogne, A. Finiels, V. Hulea, F. Fajula, Zeolite Y crystals with trimodal porosity as ideal hydrocracking catalysts, Angew. Chem. Int. Ed. 49 (2010) 10074–10078, https://doi.org/10.1002/anie.201004360.

[7] K. Na, M. Choi, R. Ryoo, Recent advances in the synthesis of hierarchically nanoporous zeolites, Microporous Mesoporous Mater. 166 (2013) 3–19, https://doi.org/10.1016/j.micromeso.2012.03.054.

[8] D. Verboekend, M. Milina, S. Mitchell, J. Pérez-Ramírez, Hierarchical zeolites by desilication: occurrence and catalytic impact of recrystallization and restructuring, Cryst. Growth Des. 13 (2013) 5025–5035, https://doi.org/10.1021/cg4010483.

[9] K. Lee, S. Lee, Y. Jun, M. Choi, Cooperative effects of zeolite mesoporosity and defect sites on the amount and location of coke formation and its consequence in deactivation, J. Catal. 347 (2017) 222–230, https://doi.org/10.1016/j.jcat.2017.01.018.

[10] C.H. Christensen, K. Johannsen, E. Törnqvist, I. Schmidt, H. Topsøe, C.H. Christensen, Mesoporous zeolite single crystal catalysts: diffusion and catalysis in hierarchical zeolites, Catal. Today 128 (2007) 117–122, https://doi.org/10.1016/j.cattod.2007.06.082.

[11] R. Chal, C. Gérardin, M. Bulut, S. van Donk, Overview and industrial assessment of synthesis strategies towards zeolites with mesopores, ChemCatChem 3 (2011) 67–81, https://doi.org/10.1002/cctc.201000158.

[12] M.S. Holm, E. Taarning, K. Egeblad, C.H. Christensen, Catalysis with hierarchical zeolites, Catal. Today 168 (2011) 3–16, https://doi.org/10.1016/j.cattod.2011.01.007.

[13] D. Verboekend, N. Nuttens, R. Locus, J. Van Aelst, P. Verolme, J.C. Groen, J. Pérez-Ramírez, B.F. Sels, Synthesis, characterisation, and catalytic evaluation of hierarchical faujasite zeolites: milestones, challenges, and future directions, Chem. Soc. Rev. 45 (2016) 3331–3352, https://doi.org/10.1039/C5CS00520E.

[14] J. Zhao, Y. Yin, Y. Li, W. Chen, B. Liu, Synthesis and characterization of mesoporous zeolite Y by using block copolymers as templates, Chem. Eng. J. 284 (2016) 405–411, https://doi.org/10.1016/j.cej.2015.08.143.

[15] J. Zhou, J. Zhao, J. Zhang, T. Zhang, M. Ye, Z. Liu, Regeneration of catalysts deactivated by coke deposition: a review, Chin. J. Catal. 41 (2020) 1048–1061, https://doi.org/10.1016/S1872-2067(20)63552-5.

[16] E.L. Moorehead, J.B. McLean, W.A. Cronkright, Microactivity evaluation of FCC catalysts in the laboratory: principles, approaches and applications, Stud. Surf. Sci. Catal. 76 (1993) 223–255, https://doi.org/10.1016/S0167-2991(08)63830-6.

[17] X. Han, H. Wang, Y. Zeng, J. Liu, Advancing the application of bio-oils by co-processing with petroleum intermediates: a review, Energy Convers. Manag. 10 (2021), 100069, https://doi.org/10.1016/j.ecmx.2020.100069.

[18] R. Bai, Y. Song, Y. Li, J. Yu, Creating hierarchical pores in zeolite catalysts, Trends Chem 1 (2019) 601–611, https://doi.org/10.1016/j.trechm.2019.05.010.

[19] G. Busca, Catalytic materials based on silica and alumina: structural features and generation of surface acidity, Prog. Mater. Sci. 104 (2019) 215–249, https://doi.org/10.1016/j.pmatsci.2019.04.003.

[20] M. Ravi, V.L. Sushkevich, J.A. van Bokhoven, Towards a better understanding of Lewis acidic aluminium in zeolites, Nat. Mater. 19 (2020) 1047–1056, https://doi.org/10.1038/s41563-020-0751-3.

[21] T. Barzetti, E. Selli, D. Moscotti, L. Forni, Pyridine and ammonia as probes for FTIR analysis of solid acid catalysts, J. Chem. Soc. Faraday. Trans. 92 (1996) 1401–1407, https://doi.org/10.1039/FT9969201401.

[22] Á. Ibarra, A. Veloso, J. Bilbao, J.M. Arandes, P. Castaño, Dual coke deactivation pathways during the catalytic cracking of raw bio-oil and vacuum gasoil in FCC conditions, Appl. Catal., B 182 (2016) 336–346, https://doi.org/10.1016/j.apcatb.2015.09.044.

[23] W. Lutz, W. Gessner, R. Bertram, I. Pitsch, R. Fricke, Hydrothermally resistant high-silica Y zeolites stabilized by covering with non-framework aluminum species, Microporous Mater. 12 (1997) 131–139, https://doi.org/10.1016/S0927-6513(97)00070-9.

[24] Y. Wei, T.E. Parmentier, K.P. de Jong, J. Zečević, Tailoring and visualizing the pore architecture of hierarchical zeolites, Chem. Soc. Rev. 44 (2015) 7234–7261, https://doi.org/10.1039/C5CS00155B.

[25] E. Koohsaryan, M. Anbia, Nanosized and hierarchical zeolites: a short review, Chin. J. Catal. 37 (2016) 447–467, https://doi.org/10.1016/S1872-2067(15)61038-5.

[26] A. Maghfirah, M.M. Ilmi, A.T.N. Fajar, G.T.M. Kadja, A review on the green synthesis of hierarchically porous zeolite, Mater. Today Chem. 17 (2020), 100348, https://doi.org/10.1016/j.mtchem.2020.100348.

[27] J.C. Groen, W. Zhu, S. Brouwer, S.J. Huynink, F. Kapteijn, J.A. Moulijn, J. Pérez-Ramírez, Direct demonstration of enhanced diffusion in mesoporous ZSM-5 zeolite obtained via controlled desilication, J. Am. Chem. Soc. 129 (2007) 355–360, https://doi.org/10.1021/ja065737o.

[28] M. Gackowski, K. Tarach, Ł. Kuterasiński, J. Podobiński, B. Sulikowski, J. Datka, Spectroscopic IR and NMR studies of hierarchical zeolites obtained by desilication of zeolite Y: optimization of the desilication route, Microporous Mesoporous Mater. 281 (2019) 134–141, https://doi.org/10.1016/j.micromeso.2019.03.004.

[29] V. Jorik, Semiempirical approach to determination of framework aluminum content in faujasite-type zeolites by X-ray powder diffraction, Zeolites 13 (1993) 187–191, https://doi.org/10.1016/S0144-2449(05)80276-3.

[30] D. Verboekend, G. Vilé, J. Pérez-Ramírez, Hierarchical Y and USY zeolites designed by post-synthetic strategies, Adv. Funct. Mater. 22 (2012) 916–928, https://doi.org/10.1002/adfm.201102411.

[31] M. Gackowski, K. Tarach, Ł. Kuterasiński, J. Podobiński, S. Jarczewski, P. Kuśtrowski, J. Datka, Hierarchical zeolites Y obtained by desilication: porosity, acidity and catalytic properties, Microporous Mesoporous Mater. 263 (2018) 282–288, https://doi.org/10.1016/j.micromeso.2017.11.051.

[32] E.G. Derouane, J.C. Védrine, R.R. Pinto, P.M. Borges, L. Costa, M.A.N.D.A. Lemos, F. Lemos, F.R. Ribeiro, The acidity of zeolites: concepts, measurements and relation to catalysis. A review on experimental and theoretical methods for the study of zeolite acidity, Catal. Rev. Sci. Eng. 55 (2013) 454–515, https://doi.org/10.1080/01614940.2013.822266.

[33] J. Fals, J.R. García, M. Falco, U. Sedran, Coke from SARA fractions in VGO. Impact on Y zeolite acidity and physical properties, Fuel 225 (2018) 26–34, https://doi.org/10.1016/j.fuel.2018.02.180.

[34] J.R. García, M. Falco, U. Sedran, Intracrystalline mesoporosity over Y zeolites: processing of VGO and resid-VGO mixtures in FCC, Catal. Today 296 (2017) 247–253, https://doi.org/10.1016/j.cattod.2017.04.010.

[35] K. Sadowska, A. Wach, Z. Olejniczak, P. Kuśtrowski, J. Datka, Hierarchic zeolites: zeolite ZSM-5 desilicated with NaOH and NaOH/tetrabutylamine hydroxide, Microporous Mesoporous Mater. 167 (2013) 82–88, https://doi.org/10.1016/j.micromeso.2012.03.045.

[36] M.S. Holm, S. Svelle, F. Joensen, P. Beato, C.H. Christensen, S. Bordiga, M. Bjørgen, Assessing the acid properties of desilicated ZSM-5 by FTIR using CO and 2,4,6-trimethylpyridine (collidine) as molecular probes, Appl. Catal., A 356 (2009) 23–30, https://doi.org/10.1016/j.apcata.2008.11.033.

[37] J.R. García, M. Bertero, M. Falco, U. Sedran, Catalytic cracking of bio-oils improved by the formation of mesopores by means of Y zeolite desilication, Appl. Catal., A 503 (2015) 1–8, https://doi.org/10.1016/j.apcata.2014.11.005.

[38] D. Wang, L. Zhang, L. Chen, H. Wu, P. Wu, Postsynthesis of mesoporous ZSM-5 zeolite by piperidine-assisted desilication and its superior catalytic properties in hydrocarbon cracking, J. Mater. Chem. 3 (2015) 3511–3521, https://doi.org/10.1039/C4TA06438K.

[39] V. Rac, V. Rakić, D. Stošić, O. Otman, A. Auroux, Hierarchical ZSM-5, beta and USY zeolites: acidity assessment by gas and aqueous phase calorimetry and catalytic activity in fructose dehydration reaction, Microporous Mesoporous Mater. 194 (2014) 126–134, https://doi.org/10.1016/j.micromeso.2014.04.003.

[40] J.R. García, C.M. Bidabehere, U. Sedran, Unsteady state diffusion-adsorption-reaction. Selectivity of consecutive reactions on porous catalyst particles, Int. J. Chem. React. Eng. 20 (2022) 83–96, https://doi.org/10.1515/ijcre-2021-0003.

[41] A. Corma, A. Chica, J.M. Guil, F.J. Llopis, G. Mabilon, J.A. Perdigón-Melón, S. Valencia, Determination of the pore topology of zeolite IM-5 by means of catalytic test reactions and hydrocarbon adsorption measurements, J. Catal. 189 (2000) 382–394, https://doi.org/10.1006/jcat.1999.2718.
[42] T. Myrstad, H. Engan, Testing of resid FCC catalysts in MAT, Appl. Catal., A 171 (1998) 161–165, https://doi.org/10.1016/S0926-860X(98)00100-8.
[43] S.H. Ng, Y. Zhu, A. Humphries, N. Nakajima, T.Y.R. Tsai, F. Ding, H. Ling, S. Yui, Key observations from a comprehensive FCC study on Canadian heavy gas oils from various origins. Part 1: yield profiles in batch reactors, Fuel Process. Technol. 87 (2006) 475–485, https://doi.org/10.1016/j.fuproc.2005.11.002.